Allosteric and ATP-Competitive Inhibitors of mTOR Effectively Suppress Tumor Progression-Associated Epithelial-Mesenchymal Transition in the Kidneys of *Tsc2*$^{+/-}$ Mice

Ashley T. Jones, Jian Yang, Kalin Narov, Elizabeth P Henske[1], Julian R. Sampson and Ming Hong Shen

Institute of Medical Genetics, Division of Cancer and Genetics, School of Medicine, Cardiff University, Heath Park, Cardiff CF14 4XN, UK

Abstract

In tuberous sclerosis (TSC)–associated tumors, mutations in the TSC genes lead to aberrant activation of the mechanistic target of rapamycin complex 1 (mTORC1) signaling pathway. mTORC1 signaling impacts many biological processes including the epithelial-mesenchymal transition (EMT), which is suggested to promote tumor progression and metastasis in various types of cancer. In this study, we report hybrid cells with epithelial and mesenchymal features in angiomyolipomas and partial EMT in carcinomas from TSC patients and describe a new model of EMT activation during tumor progression from cyst to papillary adenoma to solid carcinoma in the kidneys of *Tsc2*$^{+/-}$ mice. Features of EMT occurred infrequently in TSC-associated cysts but increased as the lesions progressed through papillary adenoma to solid carcinoma where epithelial-mesenchymal hybrid cells were abundant, indicating partial EMT. We also compared the effects of the novel ATP-competitive mTOR inhibitor AZD2014 with the allosteric mTOR inhibitor rapamycin on EMT and tumor burden. Both AZD2014 and rapamycin potently suppressed EMT of renal tumors and effectively blocked tumor progression in *Tsc2*$^{+/-}$ mice. These results suggest that partial EMT is a shared feature of TSC-associated renal tumors in humans and mice and occurs during TSC-associated tumor progression. EMT-related signaling pathways may represent therapeutic targets for tumors associated with mutations in the TSC genes.

Neoplasia (2019) 21, 731–739

Introduction

Tuberous sclerosis (TSC) is a tumor syndrome caused by mutations of the *TSC1* or *TSC2* gene [1]. Kidney lesions are one of the most frequent manifestations of TSC, with angiomyolipomas (AMLs) being the most common lesions. Despite the fact that most AMLs are benign tumors, their propensity for spontaneous hemorrhage can have life-threatening consequences. Other TSC-associated kidney lesions include oncocytoma, malignant AML, and renal cell carcinoma (RCC) [2–4]. RCC occurs in about 4% of TSC patients and is characterized by diagnosis at a young age and pathological heterogeneity with clear-cell, papillary, and chromophobe carcinoma subtypes. TSC-associated lesions are also observed in other organs including lymphangioleiomyomatosis (LAM) affecting the lungs, subependymal giant cell astrocytomas in the brain, cardiac rhabdomyomas, and facial angiofibromas. Mice heterozygous for *Tsc1*$^{+/-}$ or *Tsc2*$^{+/-}$ develop small cystic lesions in the kidneys

detectable histologically from as early as 2 months. With aging, the number and size of lesions increase, and they progress to papillary and then solid malignancies, providing a valuable model for investigating

mechanisms underlying tumor progression [5–8]. Human and mouse TSC-associated tumors show somatic loss of the corresponding second allele and aberrant activation of the mechanistic target of rapamycin complex 1 (mTORC1) signaling pathway [5,6,9,10].

mTORC1 plays a crucial role in the control of many biological activities such as cell growth, proliferation, and survival [11]. mTORC1 is also an important regulator of epithelial-mesenchymal transition (EMT) [12]. EMT is a cellular process that converts epithelial cells into cells with a mesenchymal phenotype and is coordinated by complex regulatory networks involving transcriptional control and epigenetic modifications [13,14]. EMT is critical for embryogenesis and is also implicated in wound healing and pathogenesis of disease. Activation of EMT is suggested to promote tumor initiation, progression, metastasis, and resistance to chemotherapy and immunotherapy in various types of cancer including renal cell carcinoma [15–17].

TSC-associated AML and LAM are associated with markers of EMT, although their cellular origin remains to be established [18,19]. The mesenchymal marker vimentin is also detected in some TSC-associated RCC, suggesting EMT [3]. AMLs shrink significantly in response to treatment with the allosteric mTOR inhibitor rapamycin and its derivatives [20–23], but the responses are partial, and tumors usually regrow after treatment withdrawal. Partial resistance to rapamycin or its derivatives is probably associated with loss of negative feedback regulation that leads to activation of AKT [24]. AZD2014, also known as vistusertib, is a novel ATP-competitive dual inhibitor of mTORC1 and mTORC2 and has shown dramatic suppression of EMT in hepatoma cells with significant antitumor effects in various cancer cell lines and xenograft mouse models of cancer [25–28].

In this study, we report hybrid cells with epithelial and mesenchymal features in AML and partial EMT in renal carcinomas from TSC patients and describe a new model of EMT activation during tumor progression in the kidneys of $Tsc2^{+/-}$ mice. We have also demonstrated that both AZD2014 and rapamycin effectively suppress EMT and block tumor progression. These results suggest that EMT-related signaling pathways may provide targets for treating tumors associated with mutations in the TSC genes.

Materials and Methods

Animal Procedures

Animal procedures were performed in accordance with the UK Home Office guidelines and approved by the Ethical Review Group of Cardiff University. As described previously, $Tsc2^{+/-}$ mice were backcrossed to balb/c strain [6]. To determine the effect of AZD2014 and rapamycin on EMT and molecular signaling and to compare the antitumor efficacy of AZD2014 with rapamycin, $Tsc2^{+/-}$ litter mates were randomly allocated into 3 groups of 8, balanced for gender. Animals were treated with vehicle, AZD2014 (20 mg/kg, maximum tolerated dose), and rapamycin (5 mg/kg) for 2 months from the age of 14 months through intraperitoneal injection 5 times a week. At the end of treatment, animals were humanely killed for assessment of tumor burden and analysis of protein expression and phosphorylation in normal tissues and tumor samples. AZD2014 (APExBIO, Houston, TX) at 4 mg/ml and rapamycin (LC Laboratories, Woburn, MA) at 1 mg/ml were prepared in vehicle solution (2.5% PEG-400, 2.5% Tween-80, and 2.5% DMSO) respectively.

Histology

Assessment of tumor burden in the kidneys of mice was performed as described previously [8]. Mouse kidneys were fixed in 10%

buffered formalin saline for 24 hours, processed, and paraffin embedded. Six coronal sections of 5 μm were prepared at a 200-μm interval from both kidneys of each mouse, stained with hematoxylin/eosin, and scanned using an Aperio system (http://www.aperio.com/?gclid = CNXN-8by4a UCFcINfAods3eg1w). Scanned images were used for lesion quantification using ImageJ (http://rsbweb.nih.gov/ij/). Lesion number was determined, and maximum cross-sectional whole area including noncellular spaces and cellular area of each renal lesion were measured. Tumor burdens were estimated from whole areas and cellular areas of all lesions (cystic, papillary, and solid), cystic/papillary lesions, and solid carcinomas, respectively. The assessment was conducted blindly with respect to treatment status.

Immunohistochemistry (IHC)

This study was approved by the Institutional Review Board of the Brigham and Women's Hospital, Boston MA. Human tumor sections and mouse kidney sections were prepared as described above. Conventional IHC was performed as described previously [29]. Multiple sequential IHC (MS-IHC) was performed to colocalize multiple antigens in the same cells. A crucial step of MS-IHC was to completely strip previous primary antibodies to ensure efficiency and specificity of subsequent primary antibody-antigen reactions. The protocol used for stripping primary antibodies was modified from Kim et al. [30]. For MS-IHC, previous IHC-stained slides were incubated in xylene for 10 minutes to remove coverslips and then incubated at 50°C in a buffered solution containing 5% SDS, 0.5% mercaptoethanol, and 50 mm Tris–HCl (pH 7.5) for 60 minutes to strip primary antibodies, and finally, the protocol was followed for conventional IHC. SignalStain Boost Rabbit specific IHC Detection Reagent (Cell Signaling Technology, Danvers, MA) and ImmPACT NovaRED Peroxidase Substrate or ImmPACT VIP Peroxidase (HRP) Substrate (Vector Laboratories, Peterborough, UK) were used to stain antigens according to the kit suppliers' instruction. IHC or MS-IHC stained slides were scanned to generate virtual slides for photo capture using an Aperio system. Primary antibodies were used for IHC against phosphorylated S6 ribosomal protein at S235/236, phosphorylated Akt at S473, E-cadherin, vimentin, FSP1, α-SMA (Cell Signaling Technology, Danvers, MA), Ki67, and active caspase 3 (Abcam, Cambridge, UK).

Western blot

Western blot was performed as described previously [29]. Protein extracts were prepared from normal tissues and tumor samples using AllPrep DNA/RNA/Protein Mini Kit (QIAGEN Ltd-UK, Crawley, UK). Proteins were purified according to the kit supplier's instruction. Twenty micrograms of protein per sample was separated on NuPAGE 4%-12% Bis-Tris Gels (Fisher Scientific UK Ltd., Loughborough, UK) and transferred onto Amersham Protran Premium 0.2- or 0.45-μm nitrocellulose blotting membranes (GE Healthcare UK Ltd., Little Chalfont, UK). Blots were analyzed with ECL Select Western Detection Kit (GE Healthcare UK Ltd.), and signals were detected using Autochemi Imaging System (UVP, Upland, CA). Horseradish peroxidise–conjugated secondary antibody against rabbit was used for Western blot (Cell Signaling Technology). Primary antibodies were used for Western blot against phosphorylated S6 ribosomal protein at S235/236, 4E-BP1 at T37/46, Akt at S473, Akt at T308, and E-cadherin, vimentin, β-actin (Cell Signaling Technology), phosphorylated PKC at T638 (Abcam);
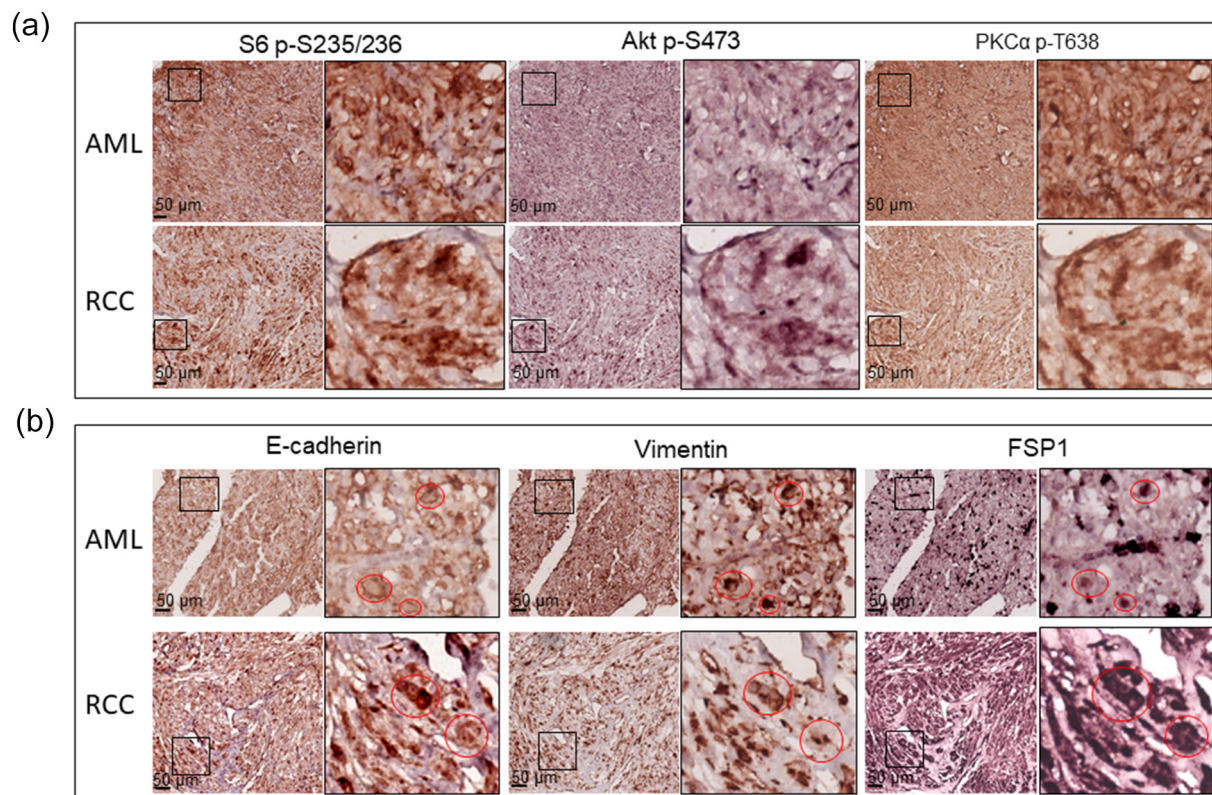
Figure 1. mTOR signaling and protein levels of epithelial and mesenchymal markers in renal lesions of TSC patients.Tumor sections prepared from TSC patients were used for MS-IHC. The same tumor sections were subjected to three rounds of IHC to sequentially detect three indicated antigens. Higher-power views of boxed areas are presented next to the corresponding lower-power images. Black lines are scale bars.(A) mTOR signaling in TSC-associated tumors. Representative IHC-stained sections were presented to show phosphorylation of S6 at S235/236, Akt at S473, and PKC at T638.(B) Expression of epithelial and mesenchymal markers in TSC-associated tumors. Representative IHC-stained sections were presented to show protein levels of E-cadherin, vimentin, and FSP1. Circled areas show examples of tumor cells co-expressing E-cadherin and vimentin/FSP1.

phosphorylated MDM2 at S166, mTOR at S2448, and mTOR at S2481 (Sigma-Aldrich, Dorset, UK).

Statistical Analysis

The Mann-Whitney test was used to compare tumor burden between treatment groups. Two-tailed Fisher's exact test was used to compare protein expression in tumor cells obtained by IHC between treatment groups. $P < .05$ was considered to be statistically significant. Analyses were performed using GraphPad Prism 7.03.

Results

Expression of Epithelial and Mesenchymal Markers in Kidney Tumors of TSC patients and Tsc2$^{+/-}$ Mice

We examined mTOR signaling and markers of epithelial and mesenchymal status in AML and RCC of TSC patients using MS-IHC. The MS-IHC technique was validated using mouse kidney sections as depicted in Supplementary Figure 1. Both mTORC1 and mTORC2 were activated in these human tumors as evidenced by increased phosphorylation of S6, Akt, and PKCα (Figure 1A). E-cadherin was used as an epithelial marker, whereas vimentin, FSP1, and α-SMA were used as mesenchymal markers. As shown in Figure 1B, vimentin and FSP1 were consistently detected in human tumors as observed previously [31], while E-cadherin expression was also

observed. Co-expression of E-cadherin and vimentin/FSP1 was observed in these tumors, indicating partial EMT in RCC and existence of hybrid cells with epithelial and mesenchymal features in AML (Figure 1B, Supplementary Figures 2 and 3). We then investigated mTOR signaling and EMT in renal lesions of Tsc2$^{+/-}$ mice using IHC on consecutive kidney sections. As reported previously [7], both mTORC1 and mTORC2 were activated in all renal lesions including cysts, papillary lesions, and solid malignancies as indicated by increased phosphorylation of S6 and Akt (Figure 2A). As shown in Figure 2A, E-cadherin was expressed in nearly all tumor cells of cystic and papillary lesions, but expression was lower, variable, and sometimes absent in tumor cells of carcinomas. In contrast, the expression of vimentin, FSP1, and α-SMA was minimal in cysts but increased in more advanced lesions (Figure 2, A and B). The IHC images from consecutive kidney sections as depicted in Figure 2A show co-expression of both epithelial and mesenchymal markers in tumor cells, suggesting partial EMT [15].To confirm this observation, MS-IHC was performed on the same kidney sections. Many hybrid epithelial-mesenchymal tumor cells were present as evidenced by co-expression of E-cadherin, vimentin, and FSP1 (Figure 2C, Supplementary Figures 4, 5, 5-1 and 5-2). These results suggest that partial EMT in TSC-associated renal tumors is a shared feature by human and mouse and that activation of EMT increases as tumors progress from cysts to papillary adenomas and solid carcinomas.
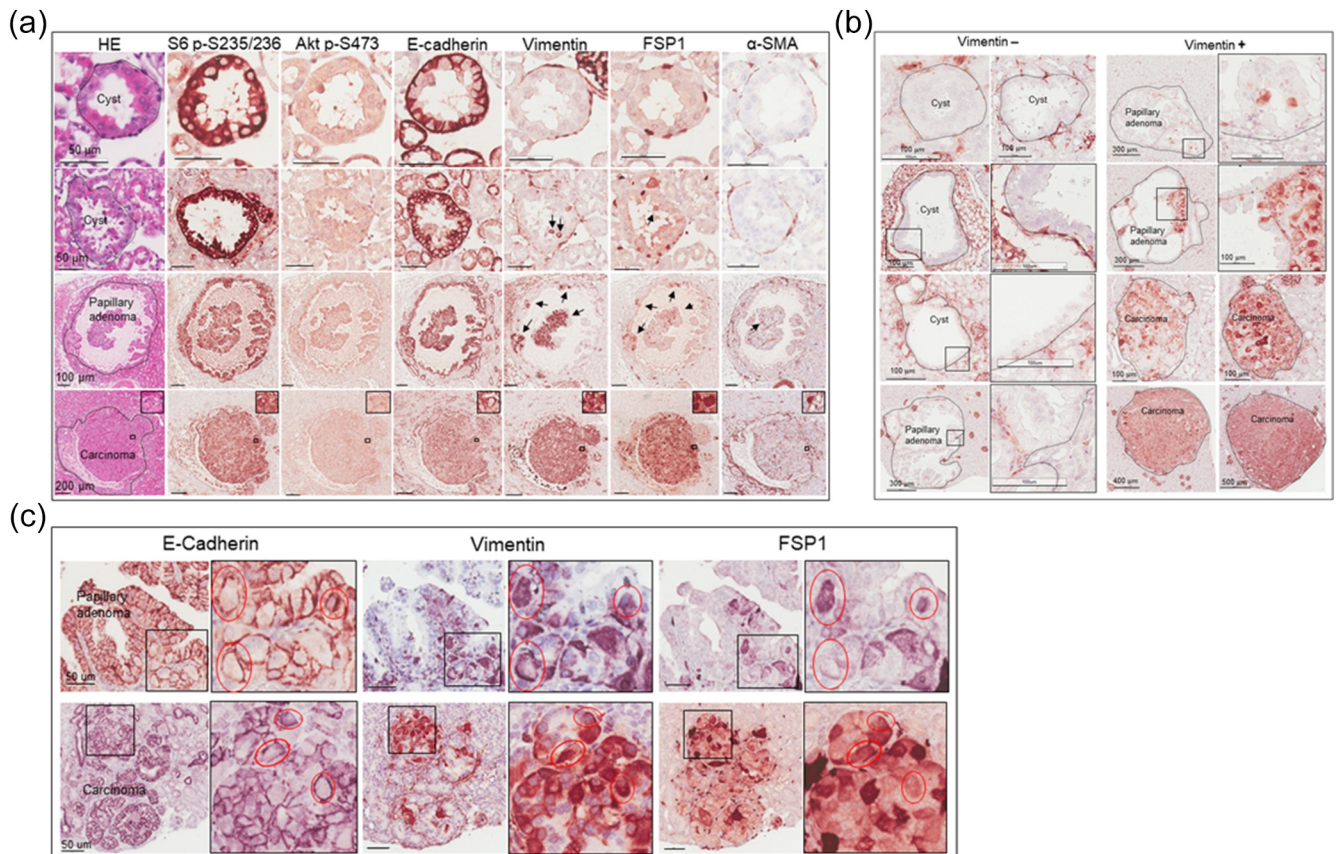
Figure 2. mTOR signaling and protein levels of epithelial and mesenchymal markers in renal lesions of $Tsc2^{+/-}$ mice.(A) mTOR signaling and expression of E-cadherin, vimentin, FSP1, and α-SMA. Adjacent kidney sections prepared from 16-month-old $Tsc2^{+/-}$ mice were used for IHC. Representative IHC-stained sections were presented to show phosphorylation of S6 at S235/236 and Akt at S473, and protein levels of E-cadherin, vimentin, FSP1, and α-SMA in different types of renal tumors from cystic/papillary lesions to solid malignancies. Black arrows point to tumor cells stained by vimentin, FSP1, or α-SMA in cystic/papillary lesions. Black lines are scale bars.(B) Expression of vimentin. Kidney sections prepared from 16-month-old $Tsc2^{+/-}$ mice were used for IHC. Representative IHC-stained sections were presented to show different types of renal tumors negative (−) or positive (+) for vimentin. Higher-power views of boxed areas are presented next to the corresponding lower-power images. Black lines are scale bars.(C) Identification of tumor cells with partial EMT. Kidney sections prepared from 16-month-old $Tsc2^{+/-}$ mice were used for MS-IHC. The same kidney sections were subjected to three rounds of IHC to sequentially detect three indicated antigens. Representative images were presented to show examples of tumor cells co-expressing E-cadherin and vimentin/FSP1 in circled areas. Higher-power views of boxed areas are presented next to the corresponding lower-power images. Around 60.1% (11.6%-96.8%) of tumor cells co-expressed E-cadherin and vimentin (and or FSP1) as estimated from 10 mouse renal carcinomas. Black lines are scale bars.

Suppression of EMT by AZD2014 and Rapamycin in Renal Tumors of $Tsc2^{+/-}$ Mice

We then asked if mTOR inhibitors suppress EMT in renal lesions. We first determined that the maximum tolerated dose of AZD2014 in $Tsc2^{+/-}$ mice was 20 mg/kg body weight per day via intraperitoneal injection in a pilot study of 2 weeks of treatment. Three groups of eight randomly allocated $Tsc2^{+/-}$ mice were then treated for 2 months, beginning at age 14 months, with vehicle, AZD2014 (20 mg/kg), or rapamycin (5 mg/kg) via intraperitoneal injection. Following treatment, we examined protein levels of E-cadherin, vimentin, and FSP1 by IHC on kidney sections. We found that the protein levels of vimentin and FSP1 were significantly attenuated in cystic/papillary lesions treated by AZD2014 or rapamycin compared to vehicle (Figure 3). The proportion of cystic/papillary lesions with one or more tumor cells positive for either vimentin or FSP1 was also significantly reduced after treatment by AZD2014 or rapamycin (Figure 3, Supplementary Tables 1 and 2). Furthermore, the protein levels of both vimentin and FSP1 were dramatically reduced in solid

carcinomas treated by AZD2014 or rapamycin compared to vehicle (Figure 4A), while the E-cadherin level was variable. Protein samples were also prepared from solid carcinomas after treatment for Western analysis. Consistently, Western analysis also demonstrated reduced vimentin and variable E-cadherin levels in solid carcinomas treated by AZD2014 or rapamycin compared to vehicle (Figure 4B). These findings suggest that both AZD2014 and rapamycin suppress EMT in most renal tumors of $Tsc2^{+/-}$ mice. However, in one large solid carcinoma from a $Tsc2^{+/-}$ mouse treated with AZD2014, protein levels of vimentin and FSP1 were not significantly affected, which were consistent with phosphorylation levels of S6 and Akt (Supplementary Figure 6), suggesting resistance to AZD2014.

Inhibition of mTORC1 and mTORC2 by AZD2014 and Rapamycin in Renal Tumors of $Tsc2^{+/-}$ Mice

We performed IHC and Western analysis to determine the effects of AZD2014 and rapamycin on mTOR signaling using kidney sections and protein samples prepared from solid carcinomas, as
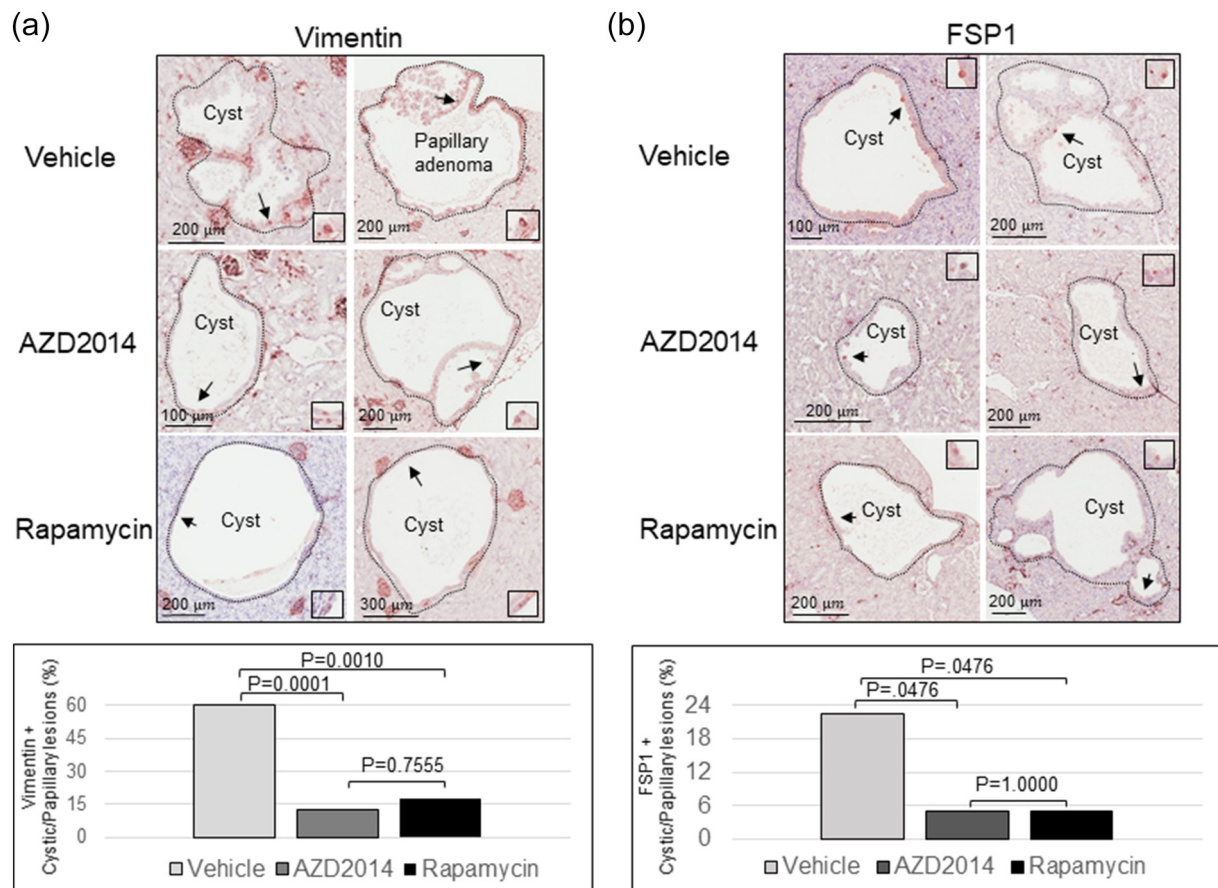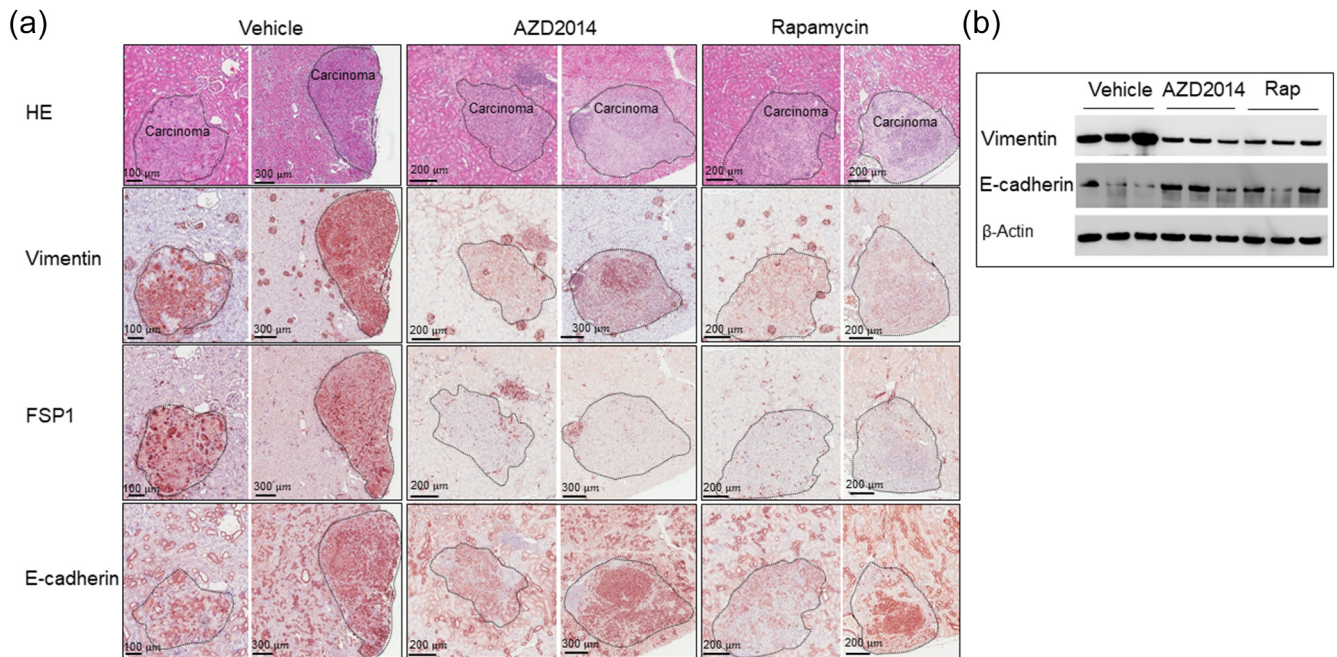
Figure 3. Effect of AZD2014 and rapamycin on EMT in cystic/papillary lesions of $Tsc2^{+/-}$ mice.(A) Kidney sections prepared from 16-month-old $Tsc2^{+/-}$ mice treated with vehicle, AZD2014, or rapamycin were used to analyze vimentin by IHC. Upper panel: Representative IHC-stained sections were presented to show protein levels of vimentin in tumor cells of cystic/papillary lesions. Black arrows point to tumor cells with detectable vimentin as shown in boxed areas. Black lines are scale bars. Bottom panel: Proportion of cystic/papillary lesions with cells positive for vimentin was shown from different treatment groups. For detailed statistical analysis, see Supplementary Tables 1 and 2.(B) Kidney sections prepared from 16-month-old $Tsc2^{+/-}$ mice treated with vehicle, AZD2014, or rapamycin were used to analyze FSP1 by IHC. Upper panel: Representative IHC-stained sections were presented to show protein levels of FSP1 in tumor cells of cystic/papillary lesions. Black arrows point to tumor cells with detectable FSP1 as shown in boxed areas. Black lines are scale bars. Bottom panel: Proportion of cystic/papillary lesions with cells positive for FSP1 was shown from different treatment groups.

described above. Phosphorylation of mTOR at S2448, S6 at s235/236, and 4E-BP1 at T37/46 was used as readouts of mTORC1 activity, and phosphorylation of mTOR at S2481, Akt at S473 and T450, PKCα at T638, and the Akt substrate MDM2 at S166 was used as readouts of mTORC2 activity. As expected, AZD2014 markedly reduced phosphorylation of all mTORC1 and mTORC2 markers in all renal tumors and normal kidneys (Figure 5, Supplementary Figure 7). AZD2014 also reduced phosphorylation of Akt at T308 (Figure 5B). Rapamycin significantly reduced phosphorylation of all mTORC1 markers in all renal tumors and normal kidneys (Figure 5, Supplementary Figure 7). In addition, rapamycin clearly decreased phosphorylation of mTOR at S2481, PKCα at T638, and MDM2 at S166 in solid tumors (Figure 5) and of mTOR at S2481, and Akt at S473 and T450 in normal kidney tissues (Supplementary Figure 7), but effects of rapamycin on phosphorylation of Akt at T308 and S473 appeared to be variable in solid carcinomas (Figure 5). As expected, increased phosphorylation of Akt at S473 was also observed in some cystic lesions treated by rapamycin (Figure 5A) as described previously [29], while other lesions did not show evidence of rapamycin-induced increase in phosphorylation of Akt at S473. These results indicate that

AZD2014 potently inhibited mTORC1 and mTORC2, while rapamycin inhibited mTORC1 potently but partially inhibited mTORC2 in renal tumors.

Effective blocking of Tumor Progression by AZD2014 and Rapamycin in the kidneys of Tsc2$^{+/-}$ Mice

Both AZD2014 and rapamycin strikingly inhibited proliferation of tumor cells in the kidneys of $Tsc2^{+/-}$ mice, but no significant changes in apoptosis were detected with either drug given individually (Supplementary Figure 8). We therefore sought to compare the antitumor efficacy of AZD2014 with rapamycin in $Tsc2^{+/-}$ mice. Animals treated for 2 months as described above were used for tumor burden assessment. All animals survived until termination of treatment, and no animals showed significant weight loss or other observable clinical signs. Tumor burden was determined by analyzing all lesions (cystic/papillary/solid), cystic/papillary lesions, and solid carcinomas in the kidneys, respectively. Both AZD2014 and rapamycin significantly reduced the total number ($P = .0012$; $P = .0002$), size ($P = .0047$; $P = .0047$), and cellular area ($P = .0047$; $P = .0002$) of all lesions (Figure 6, Supplementary Table 3). Similarly, both AZD2014 and rapamycin significantly reduced the
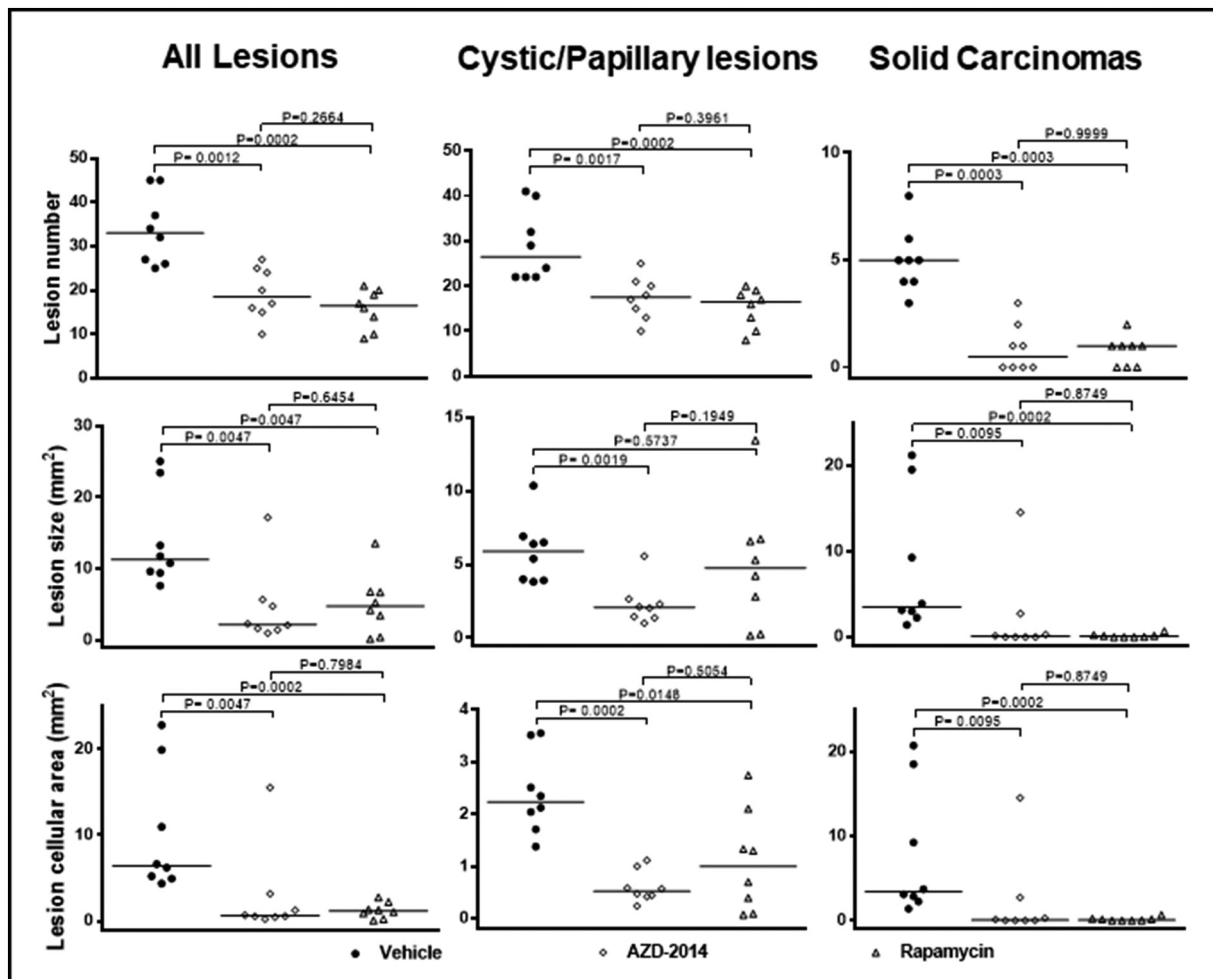
Figure 4. Effect of AZD2014 and rapamycin on EMT in solid tumors of $Tsc2^{+/-}$ mice.(A) IHC analysis. Adjacent kidney sections prepared from 16-month-old $Tsc2^{+/-}$ mice treated with vehicle, AZD2014, or rapamycin were used to analyze EMT by IHC. Representative IHC-stained images were presented to show protein levels of vimentin, FSP1, and C-cadherin in solid tumors. Black lines are scale bars.(B) Western blot analysis. Proteins were prepared from solid carcinomas dissected from $Tsc2^{+/-}$ mice treated for 2 months from the age of 14 months with vehicle, AZD2014, or rapamycin. Beta-actin was used as a loading control. Representative Western blots were presented to show expression levels of vimentin and E-cadherin.

total number (P = .0017; P = .0002) and cellular area (P = .0002; P = .0148) of cystic/papillary lesions (Figure 6, Supplementary Table 4). AZD2014 significantly reduced the total size of cystic/ papillary lesions (P = .0019). Rapamycin also appeared to reduce the total size of cystic/papillary lesions but not statistically significant (P = .5737). Further, both AZD2014 and rapamycin significantly
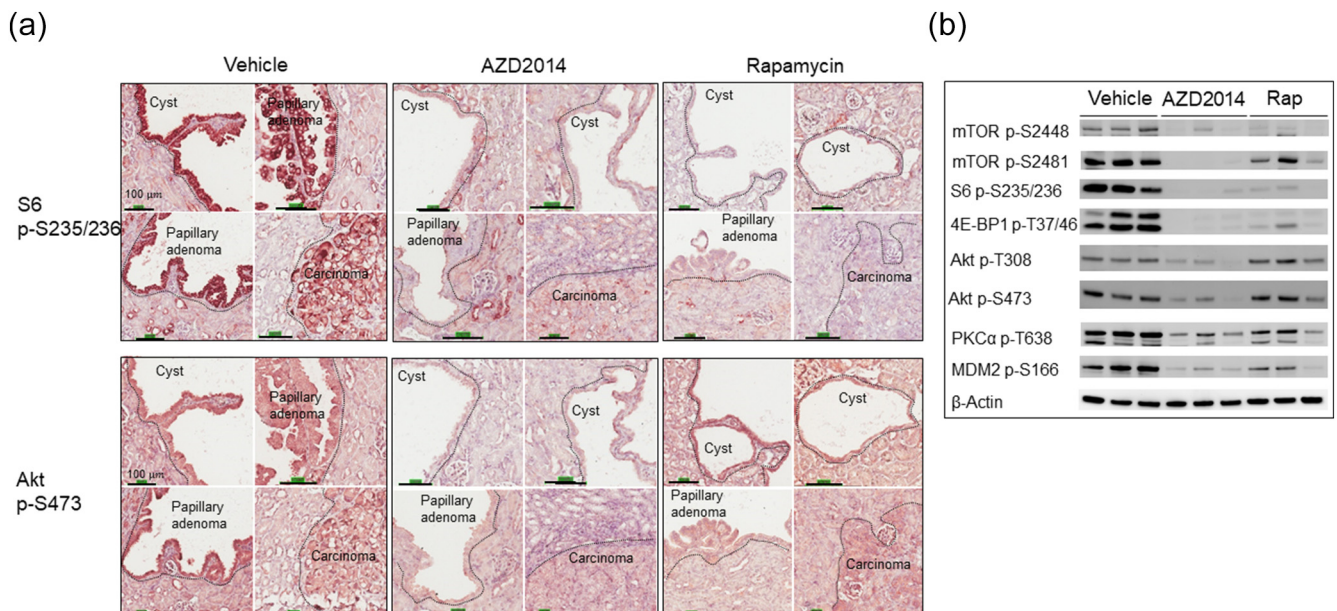
Figure 5. Effect of AZD2014 and rapamycin on mTORC1 and mTORC2 in renal tumors of $Tsc2^{+/-}$ mice.(A) IHC analysis. Adjacent kidney sections prepared from 16-month-old $Tsc2^{+/-}$ mice treated with vehicle, AZD2014, or rapamycin were used for IHC analysis. Representative IHC-stained sections were presented to show phosphorylation of mTOR at S6 at S235/236 and Akt at S473 in renal tumors. Black lines are scale bars.(B) Western blot analysis. Proteins were prepared from solid carcinomas dissected from $Tsc2^{+/-}$ mice treated for 2 months from the age of 14 months with vehicle, AZD2014, or rapamycin. Beta-actin was used as a loading control. Representative Western blots were presented to show phosphorylation of mTOR at S2448 and S2481, S6 at S235/236, 4E-BP1 at T37/46, Akt at T308 and S473, PKCα at T638, and MDM2 at S166.

Figure 6. Efficacy of AZD2014 and rapamycin on renal tumors in $Tsc2^{+/-}$ mice.$Tsc2^{+/-}$ mice were treated from 14 months old for 2 months (n = 8 each group). Dosages are described in methods. After treatment, kidney sections were prepared for histological assessment of treatment efficacy. Left panel: comparison of total number and size (area) as well as cellular area of all lesions (cystic, papillary and solid). Middle panel: comparison of total number and size (area) as well as cellular area of cystic/papillary lesions. Right panel: comparison of total number and size (area) as well as cellular area of solid carcinomas. Horizontal bars indicate a median. For detailed statistical analysis, see Supplementary Tables 3–5.

reduced total number (P = .0003; P = .0003), size (P = .0095; P = .0002), and cellular area (P = .0095; P = .0002) of solid carcinomas (Figure 6, Supplementary Table 5). No significant difference in antitumor efficacy was found between AZD2014 and rapamycin. These results indicate that both AZD2014 and rapamycin effectively block tumor progression in the kidneys of $Tsc2^{+/-}$ mice.

Discussion

We examined epithelial and mesenchymal markers in renal tumors from TSC patients and $Tsc2^{+/-}$ mice. We observed partial EMT in TSC-RCC, and hybrid cells with epithelial and mesenchymal features in AML from TSC patients. EMT in sporadic RCC has been associated with poor prognosis [32], and vimentin expression was previously reported in TSC-associated RCC [3]. TSC-associated renal AML and pulmonary LAM cells are considered to be mesenchymal tumors, but their origin remains to be established. EMT has been suggested to contribute to the pathogenesis of these lesions [18,19,33]. Our findings in TSC-associated human tumors are consistent with these observations. We also found that features consistent with partial

EMT developed during tumor progression from cysts to papillary adenomas and solid carcinomas in $Tsc2^{+/-}$ mice. Partial EMT, but not necessarily complete EMT, is implicated in tumor progression and metastasis, and tumor cells undergoing partial EMT appear to have some attributes of cancer stem cells [15,16,34–38]. The hybrid or intermediate epithelial-mesenchymal states of partial EMT observed in circulating tumor cells of cancer patients may confer plasticity and facilitate reverse mesenchymal-epithelial transition that is required for metastatic colonization [37].

Until recently, most EMT-related studies to improve our understanding of the mechanisms underlying tumor progression and metastasis were performed in cultured tumor cells or in xenograft tumor models. In a transgenic mouse model of pancreatic cancer, the intermediate epithelial-mesenchymal states were determined by lineage tracking through a $Pdx1\text{-}Cre; Rosa^{YFP}$ system in premalignant lesions and circulating pancreatic epithelial cells with attributes of cancer stem cells [34]. Recently, several studies have also used lineage tracking to determine EMT status to assess the roles of EMT-inducing transcription factors in tumor progression and metastasis in transgenic mouse models. These studies suggested that the

contribution of EMT to cancer progression/metastasis and resistance to therapy depends on tumor type and tissue origin [39–41] . In the current study, we used MS-IHC to directly characterize individual tumor cells that co-express epithelial and mesenchymal markers during tumor progression, from cystic lesions to papillary adenomas and solid carcinomas, in the kidneys of $Tsc2^{+/-}$ mice. Based on our data, we propose a new model of EMT activation during tumor progression.

Most tumors in patients with TSC are benign (and often classified as hamartomas). Nonetheless, malignant and metastatic variants of TSC-associated RCC and malignant AML can develop, and a metastatic mechanism also appears to be involved in the pathogenesis in $TSC2$-associated pulmonary LAM [42]. Lung metastasis can occur from renal cancers in $Tsc1^{+/-}$ mice, while there is little evidence of metastatic disease from renal tumors in $Tsc2^{+/-}$ mice [5]. It may be interesting, therefore, to investigate the relationship of EMT to LAM [33] and to tumor progression and lung metastasis in $Tsc1^{+/-}$ mice.

We and others previously reported that rapamycin and ATP-competitive PI3K/mTOR dual inhibitors such as GSK2126458 and NVP-BEZ235 are effective for treating renal tumors in $Tsc2^{+/-}$ mice [29,43]. In the current study, we compared the therapeutic efficacy of AZD2014 (an ATP-competitive dual inhibitor of mTORC1/mTORC2) and rapamycin for renal tumors in these mice and found that both agents effectively reduced tumor burden. As expected, AZD2014 consistently inhibited both mTORC1 and mTORC2, while rapamycin strongly inhibited mTORC1 but exhibited only a partial inhibitory effect on mTORC2 [27–29]. Tumor cells insensitive to rapamycin were reported to be sensitive to AZD2014 *in vitro* [44,45]. AZD2014 also enhanced the radiosensitivity of glioblastoma stem-like cells *in vitro* and *in vivo* in a preclinical study [46]. In a xenograft mouse model of renal carcinoma, AZD2014 was reported to be a more effective treatment than rapamycin [28]. In contrast, we did not observe any superiority of AZD2014 over rapamycin in antitumor efficacy, possibly reflecting differences in tumor types and model systems. In a first-in-human pharmacokinetic and pharmacodynamic study, partial responses to AZD2014 were seen in a patient with pancreatic cancer and a patient with breast cancer [47]. However, a recent randomized phase 2 clinical trial suggested that AZD2014 was not as effective as everolimus (a rapamycin derivative) for VEGF-refractory metastatic clear cell renal cancer [48]. Combination of AZD2014 with other antitumor agents may improve therapeutic efficacy as described in preclinical models of various malignancies [49]. Over 20 clinical trials of cancer treatment have been initiated using combination therapy of AZD2014 with other antitumor agents in the last year (https://clinicaltrials.gov/ct2/results?cond=azd2014&term=&cntry1=&state1=&recrs=). To date, there are no reports of treatment of TSC patients using ATP-competitive PI3K/mTOR inhibitors, but a clinical trial has recently been planned to treat patients with $TSC1/2$ mutated refractory solid cancers using AZD2014 (https://www.findmecure.com/clinicaltrials/show/nct03166176). Considering the promising but partial response of TSC-associated tumors to rapamycin or its derivatives [20–23], further studies are warranted to compare the therapeutic efficacy of AZD2014 with rapamycin or its derivatives in clinical settings.

In conclusion, we have established that both AZD2014 and rapamycin suppress EMT and reduce the burden of all types of renal tumors in $Tsc2^{+/-}$ mice. We identified only a single large solid tumor that was resistant to AZD2014. Suppression of EMT may contribute to the antitumor efficacy of these agents for TSC-associated tumors. Liao et al. reported that both AZD2014 and rapamycin suppressed EMT in hepatoma cells, with AZD2014 having stronger effects [26]. Torin 1 (another ATP-competitive mTORC1/mTORC2 inhibitor) and rapamycin also suppressed EMT in glioblastoma cells [50]. EMT is activated and controlled through multiple complex regulatory networks in tumors [13,14]. Targeting these networks in combination with mTOR inhibition may provide opportunities for the therapy of refractory tumor types and eradication of cancer stem cells. Further studies are required for the full dissection of the signaling pathways involved in EMT in TSC-associated tumors, including further investigation of TGFβ signaling, a potent driver of EMT and tumor progression.

Supplementary data to this article can be found online at https://doi.org/10.1016/j.neo.2019.05.003.

Conflict of Interest Statement

The authors declare no conflict of interest.

Acknowledgements

References

[1] Consortium ECTS (1993). Identification and characterization of the tuberous sclerosis gene on chromosome 16. *Cell* **75**(7), 1305–1315.

[2] Bjornsson J, Short MP, and Kwiatkowski DJ (1996 Oct). Henske EP tuberous sclerosis-associated renal cell carcinoma. Clinical, pathological, and genetic features. *Am J Pathol* **149**(4), 1201–1208.

[3] Yang P, Cornejo KM, Sadow PM, Cheng L, Wang M, and Xiao Y, et al (2014). Renal cell carcinoma in tuberous sclerosis complex. *Am J Surg Pathol* **38**(7), 895–909.

[4] Guo J, Tretiakova MS, Troxell ML, Osunkoya AO, Fadare O, Sangoi AR, Shen SS, Lopez-Beltran A, Mehra R, and Heider A, et al (2014 Nov). Tuberous sclerosis-associated renal cell carcinoma: a clinicopathologic study of 57 separate carcinomas in 18 patients. *Am J Surg Pathol* **38**(11), 1457–1467.

[5] Wilson C, Idziaszczyk S, Parry L, Guy C, Griffiths DF, and Lazda E, et al (2005). A mouse model of tuberous sclerosis 1 showing background specific early post-natal mortality and metastatic renal cell carcinoma. *Hum Mol Genet* **14**(13), 1839–1850.

[6] Onda H, Lueck A, Marks PW, Warren HB, and Kwiatkowski DJ (1999). Tsc2 (+/−) mice develop tumors in multiple sites that express gelsolin and are influenced by genetic background. *J Clin Investig* **104**(6), 687–695.

[7] Yang J, Kalogerou M, Samsel PA, Zhang Y, Griffiths DF, and Gallacher J, et al (2015). Renal tumours in a Tsc2(+/−) mouse model do not show feedback inhibition of Akt and are effectively prevented by rapamycin. *Oncogene* **34**(7), 922–931.

[8] Kalogerou M, Zhang Y, Yang J, Garrahan N, Paisey S, and Tokarczuk P, et al (2012). T2 weighted MRI for assessing renal lesions in transgenic mouse models of tuberous sclerosis. *Eur J Radiol* **81**(9), 2069–2074.

[9] Henske EP, Wessner LL, Golden J, Scheithauer BW, Vortmeyer AO, Zhuang Z, Klein-Szanto AJ, and Kwiatkowski DJ (1997 Dec). Yeung RS Loss of tuberin in both subependymal giant cell astrocytomas and angiomyolipomas supports a two-hit model for the pathogenesis of tuberous sclerosis tumors. *Am J Pathol* **151**(6), 1639–1647.

[10] Tyburczy ME, Jozwiak S, Malinowska IA, Chekaluk Y, Pugh TJ, Wu CL, Nussbaum RL, Seepo S, Dzik T, and Kotulska K, et al (2015 Apr 1). A shower of second hit events as the cause of multifocal renal cell carcinoma in tuberous sclerosis complex. *Hum Mol Genet* **24**(7), 1836–1842.

[11] Guertin DA and Sabatini DM (2007). Defining the role of mTOR in cancer. *Cancer Cell* **12**(1), 9–22.

[12] Lamouille S, Xu J, and Derynck R (2014). Molecular mechanisms of epithelial-mesenchymal transition. *Nat Rev Mol Cell Biol* **15**(3), 178–196.

[13] Kalluri R and Weinberg RA (2009). The basics of epithelial-mesenchymal transition. *J Clin Invest* **119**(6), 1420–1428.

[14] Thiery JP, Acloque H, Huang RY, and Nieto MA (2009). Epithelial-mesenchymal transitions in development and disease. *Cell* **139**(5), 871–890.

[15] Nieto MA, Huang RY, Jackson RA, and Thiery JP (2016). EMT: 2016. *Cell* **166**(1), 21–45.

[16] Lambert AW, Pattabiraman DR, and Weinberg RA (2017). Emerging biological principles of metastasis. *Cell* **168**(4), 670–691.

[17] Piva F, Giulietti M, Santoni M, Occhipinti G, Scarpelli M, and Lopez-Beltran A, et al (2016). Epithelial to mesenchymal transition in renal cell carcinoma: implications for cancer therapy. *Mol Diagn Ther* **20**(2), 111–117.

[18] Barnes EA, Kenerson HL, Jiang X, and Yeung RS (2010 Oct). Tuberin regulates E-cadherin localization. *implications in epithelial-mesenchymal transition Am J Pathol* **177**(4), 1765–1778.

[19] Bi XG, Guo L, Wang XL, Wei Q, Du Q, Jiang WH, Zheng GY, Zhang HT, Ma JH, and Zheng S (2017 Jul). Distinct subcellular localization of E-cadherin between epithelioid angiomyolipoma and triphasic angiomyolipoma: a preliminary case-control study. *Oncol Lett* **14**(1), 695–704.

[20] Bissler J, McCormack F, Young L, Elwing J, Chuck G, and Leonard J, et al (2008). Sirolimus for angiomyolipoma in tuberous sclerosis complex or lymphangioleiomyomatosis. *N Engl J Med* **358**(2), 140–151.

[21] Davies D, De Vries P, Johnson S, McCartney D, Cox J, and Serra A, et al (2011). Sirolimus therapy in tuberous sclerosis or sporadic lymphangioleiomyomatosis. *Clin Cancer Res* **17**(12), 4071–4081.

[22] Bissler JJ, Kingswood JC, Radzikowska E, Zonnenberg BA, Frost M, and Belousova E, et al (2013). Everolimus for angiomyolipoma associated with tuberous sclerosis complex or sporadic lymphangioleiomyomatosis (EXIST-2): a multicentre, randomised, double-blind, placebo-controlled trial. *The Lancet* **381**(9869), 817–824.

[23] Kim H, Kim ST, Kang SH, Sung DJ, Kim CH, and Shin SW, et al (2014). The use of everolimus to target carcinogenic pathways in a patient with renal cell carcinoma and tuberous sclerosis complex- a case report. *J Med Case Reports* **8**(10).

[24] O'Reilly KE, Rojo F, She QB, Solit D, Mills GB, and Smith D, et al (2006). mTOR inhibition induces upstream receptor tyrosine kinase signaling and activates Akt. *Cancer Res* **66**(3), 1500–1508.

[25] Pike KG, Malagu K, Hummersone MG, Menear KA, Duggan HM, and Gomez S, et al (2013). Optimization of potent and selective dual mTORC1 and mTORC2 inhibitors: the discovery of AZD8055 and AZD2014. *Bioorg Med Chem Lett* **23**(5), 1212–1216.

[26] Liao H, Huang Y, Guo B, Liang B, Liu X, and Ou H, et al (2014). Dramatic antitumor effects of the dual mTORC1 and mTORC2 inhibitor AZD2014 in hepatocellular carcinoma. *Am J Cancer Res* **5**(1), 125–139.

[27] Guichard SM, Curwen J, Bihani T, D'Cruz CM, Yates JW, and Grondine M, et al (2015). AZD2014, an inhibitor of mTORC1 and mTORC2, is highly effective in ER+ breast cancer when administered using intermittent or continuous schedules. *Mol Cancer Ther* **14**(11), 2508–2518.

[28] Zheng B, Mao JH, Qian L, Zhu H, Gu DH, and Pan XD, et al (2015). Preclinical evaluation of AZD-2014, a novel mTORC1/2 dual inhibitor, against renal cell carcinoma. *Cancer Lett* **357**(2), 468–475.

[29] Narov K, Yang J, Samsel PA, Jones A, Sampson JR, and Shen M (2017). The dual PI3KmTOR inhibitor GSK2126458 is effective for treating solid renal tumours in Tsc2+- mice through suppression of cell proliferation and induction of apoptosis. *Oncotarget* **8**(35), 58504–58512.

[30] Kim M, Soontornniyomkij V, Ji B, and Zhou X (2012). System-wide immunohistochemical analysis of protein co-localization. *PloS one* **7**(2)e32043.

[31] Karbowniczek M, Yu J, and Henske EP (2003). Renal angiomyolipomas from patients with sporadic lymphangiomyomatosis contain both neoplastic and non-neoplastic vascular structures. *Am J Pathol* **162**(2), 491–500.

[32] Piva F, Giulietti M, Santoni M, Occhipinti G, Scarpelli M, Lopez-Beltran A, Cheng L, Principato G, and Montironi R (2016). Epithelial to mesenchymal transition in renal cell carcinoma: implications for cancer therapy. *Mol Diagn Ther* **20**(2), 111–7.

[33] Gu X, Yu JJ, Ilter D, Blenis N, Henske EP, and Blenis J (2013). Integration of mTOR and estrogen-ERK2 signaling in lymphangioleiomyomatosis pathogenesis. *Proc Natl Acad Sci U S A* **110**(37), 14960–14965.

[34] Rhim AD, Mirek ET, Aiello NM, Maitra A, Bailey JM, and McAllister F, et al (2012). EMT and dissemination precede pancreatic tumor formation. *Cell* **148**(1–2), 349–361.

[35] Schliekelman MJ, Taguchi A, Zhu J, Dai X, Rodriguez J, and Celiktas M, et al (2015). Molecular portraits of epithelial, mesenchymal, and hybrid States in lung adenocarcinoma and their relevance to survival. *Cancer Res* **75**(9), 1789–1800.

[36] Jolly M, Tripathi S, Jia D, Mooney S, Celiktas M, and Hanash S, et al (2016). Stability of the hybrid epithelialmesenchymal phenotype. *Oncotarget* **7**(19), 27067–27084.

[37] Lecharpentier A, Vielh P, Perez-Moreno P, Planchard D, Soria JC, and Farace F (2011). Detection of circulating tumour cells with a hybrid (epithelial/mesenchymal) phenotype in patients with metastatic non–small cell lung cancer. *Br J Cancer* **105**(9), 1338–1341.

[38] Yu M, Bardia A, Wittner B, Stott S, Smas M, and Ting D, et al (2013). Circulating breast tumor cells exhibit dynamic changes in epithelial and mesenchymal composition. *Science* **339**(6119), 580–584.

[39] Ye X, Tam WL, Shibue T, Kaygusuz Y, Reinhardt F, and Ng Eaton E, et al (2015). Distinct EMT programs control normal mammary stem cells and tumour-initiating cells. *Nature* **525**(7568), 256–260.

[40] Fischer KR, Durrans A, Lee S, Sheng J, Li F, and Wong ST, et al (2015). Epithelial-to-mesenchymal transition is not required for lung metastasis but contributes to chemoresistance. *Nature* **527**(7579), 472–476.

[41] Zheng X, Carstens JL, Kim J, Scheible M, Kaye J, and Sugimoto H, et al (2015). Epithelial-to-mesenchymal transition is dispensable for metastasis but induces chemoresistance in pancreatic cancer. *Nature* **527**(7579), 525–530.

[42] Henske EP and McCormack FX (2012). Lymphangioleiomyomatosis — a wolf in sheep's clothing. *J Clin Invest* **122**(11), 3807–3816.

[43] Pollizzi K, Malinowska-Kolodziej I, Stumm M, Lane H, and Kwiatkowski D (2009). Equivalent benefit of mTORC1 blockade and combined PI3K-mTOR blockade in a mouse model of tuberous sclerosis. *Mol Cancer* **8**, 38.

[44] Vandamme T, Beyens M, de Beeck KO, Dogan F, van Koetsveld PM, and Pauwels P, et al (2016). Long-term acquired everolimus resistance in pancreatic neuroendocrine tumours can be overcome with novel PI3K-AKT-mTOR inhibitors. *Br J Cancer* **114**(6), 650–658.

[45] Kim ST, Kim SY, Klempner SJ, Yoon J, Kim N, and Ahn S, et al (2017). Rapamycin-insensitive companion of mTOR (RICTOR) amplification defines a subset of advanced gastric cancer and is sensitive to AZD2014-mediated mTORC1/2 inhibition. *Annals of oncology : official journal of the European Society for Medical Oncology* **28**(3), 547–554.

[46] Kahn J, Hayman TJ, Jamal M, Rath BH, Kramp T, and Camphausen K, et al (2014). The mTORC1/mTORC2 inhibitor AZD2014 enhances the radiosensitivity of glioblastoma stem-like cells. *Neuro Oncol* **16**(1), 29–37.

[47] Basu B, Dean E, Puglisi M, Greystoke A, Ong M, and Burke W, et al (2015). First-in-human pharmacokinetic and pharmacodynamic study of the dual mTORC 1/2 inhibitor AZD2014. *Clin Cancer Res* **21**(15), 3412–3419.

[48] Powles T, Wheater M, Din O, Geldart T, Boleti E, and Stockdale A, et al (2015). A randomised phase 2 study of AZD2014 versus everolimus in patients with VEGF-refractory metastatic clear cell renal cancer. *Eur Urol* **69**(3), 450–456.

[49] Singleton KR, Hinz TK, Kleczko EK, Marek LA, Kwak J, and Harp T, et al (2015). Kinome RNAi screens reveal synergistic targeting of MTOR and FGFR1 pathways for treatment of lung cancer and HNSCC. *Cancer Res* **75**(20), 4398–4406.

[50] Catalano M, D'Alessandro G, Lepore F, Corazzari M, Caldarola S, and Valacca C, et al (2015). Autophagy induction impairs migration and invasion by reversing EMT in glioblastoma cells. *Mol Oncol* **9**(8), 1612–1625.